Environmental Engineering and Management Journal

March 2019, Vol.18, No.3, 693-705
http://www.eemj.icpm.tuiasi.ro/; http://www.eemj.eu

"Gheorghe Asachi" Technical University of Iasi, Romania

ADSORPTION OF PHENOL ON ADSORBENTS PRODUCED FROM COCONUT TREE WASTE: KINETIC AND EQUILIBRIUM STUDIES

Marta Duarte*, Graziele Nascimento, Maressa Santos, Thiago Silva, Natália Campos, Jean Santos, Celmy Barbosa

Federal University of Pernambuco, Chemical Engineering Department, Avenida Artur de Sá, s/n, 50740-521 Recife, Brazil

Abstract

Agro-industrial waste are seen as potential precursors in the development of adsorbents for the removal of phenolic compounds, which exhibit a harmful effect to human health due to their high toxicity. This work evaluated the use of coal prepared from coconut tree agro-industrial waste, for the adsorption of phenol in aqueous solutions. Three coal samples were prepared as follows: carbonized only (C_b), activated with synthetic air (C_{air}) and activated with CO_2 (C_{CO2}). Based on the results of characterization, it was observed that these adsorbents are mesoporous, with a predominantly amorphous structure. The C_{CO2} demonstrated the highest thermal stability. Based on pH_{PZC}, it was found that after the activation process, the surface of the material became positively charged at a higher pH range of the solution; therefore, favouring the adsorption of phenol. In the kinetic study the pseudo-nth order model obtained the best adjustment to the experimental data. The intra-particle diffusion model indicated that the adsorption processes are controlled by various steps. The experimental data of the equilibrium adsorption study were also evaluated; with no significant difference being found between the models that were better adjusted (Fritz-Schlunder, Redlich-Peterson, Radke-Prausnitz and Sips) according to the F-test at a 95% confidence level. The maximum adsorptive capacity for C_b, C_{air} and C_{CO2} were of 32, 41 and 56 mg g^{-1}, respectively. In this study, the coconut tree straw, an abundant agro-industrial residue that has not been previously evaluated as a precursor for the preparation of coal was valued being used as an adsorbent in the removal of phenol.

Keywords: adsorption, agro-industrial residues, coconut tree straw, phenol

Received: February, 2016; Revised final: June, 2016; Accepted: August, 2016; Published in final edited form: March, 2019

1. Introduction

The cultivation of coconut tree has intensified over the past years, being commercially traded in approximately 90 countries, aiming at meeting the growing demand for coconut-derived products. In Brazil, the coconut tree is cultivated in order to produce fruits for the agro-industry (Martins and Jesus Júnior, 2014). The cultivation of coconut tree, traditionally takes place in Northeastern Brazil, where 202,309 hectares of coconut are cultivated (IBGE, 2017), resulting in an annual production of 1.5 million tonnes of residues. From this total, 600,000 tonnes consist of coconut tree straw, with low or no economic value, and its disposal may lead to environmental problems (Ageitec, 2010). The agro-industrial residues, such as coconut tree straw, are considered a promising low-cost organic matter, being highly used in the production of activated carbon (Gundogdu, 2012). The use of activated carbon produced from agro-industrial residues can settle environmental problems such as: waste accumulation, air and water pollution, besides adding economic value to the residues (Rincón-Silva et al., 2015).

Some activated carbons prepared from agro-industrial waste, such as babassu coconut shell and dende coconut shell (Couto Jr et al., 2015), nut shell (Lekene et al., 2015), Eucalyptus seed (Rincón-Silva et al., 2015), coconut shells (Zhang et al., 2016; Karri et al., 2017), peanut shells (Gama at el., 2018), rice husk (Fu et al., 2019), sawdust (Sellaoui et al., 2019) have been evaluated in terms of their effectiveness in

*Author to whom all correspondence should be addressed: e-mail: marta.duarte@ufpe.br; Phone: +55 8121267291; Fax: +55 8121267278

removing organics compounds. Among these compounds, the phenolic compounds are classified as priority pollutants, due to their high toxicity and poor biodegradability (Rodrigues et al., 2011; Saraç et al., 2017). The presence of phenolic compounds in sublethal doses affects the nervous and circulatory systems, thereby reducing blood cell growth (Britto and Rangel, 2008). Besides that, the consumption of phenol-contaminated water can damage human kidneys, the liver and pancreas (Păcurariu et al., 2013).

The phenolic compounds present in industrial effluents from the chemical, pharmaceutical, paper, wood, rubber, dye, pesticide, petroleum and gas industries must be removed before the effluents being discarded in the receiver body or reused (Kulkarni et al., 2013; Sun et al., 2019). Phenol is removed from waste water by photocatalytic degradation (Karthikeyan and Gopalakrishnan, 2017), biological treatment (Almasi et al., 2018), biodegradation (Saraç et al., 2017) and adsorption (Luo et al., 2017).

Adsorptive methods are characterized by their insensitivity to toxic substances, the simplicity of their design and operation, as well as their easiness of regeneration and low cost. Activated carbon as adsorbent has favourable characteristics such as selectivity, adsorption capacity and regeneration (Soto et al., 2011; Secula et al., 2018). The characteristics of the activated carbon arise from the properties of the raw materials and the activation method (Couto et al., 2012). The methods used for the production of activated carbon can be divided into two categories: the physical and chemical activation. In the chemical activation, the raw material is impregnated with an activation agent, and afterwards thermally treated. In the physical activation, the most commercially widespread, the raw material is first carbonized, with the carbonized material being then activated with steam, carbon dioxide, synthetic air or its mixtures (Jun et al., 2010).

This article refers to the use of the activated carbon produced from the coconut tree straw, an abundant agro-industrial residue not previously used as an adsorbent in the removal of phenol in aqueous solution. In the trials non-activated carbons and carbons activated with synthetic air and CO_2 were used. The experimental data of the kinetic and equilibrium analysis were confronted in several models.

2. Experimental

2.1. Preparation of the adsorbents

The charcoal used in this study was obtained from a coconut tree straw donated by the Elephant Chemical Industry Ltda. and activated with synthetic air (80% N_2 and 20% O_2) or CO_2. The charcoal was activated in an electric furnace (Lindberg, Blue M). Samples of 50 g of charcoal were placed in a cylindrical quartz reactor. The sample was heated from room temperature (298 ± 1K) to 873 K under a nitrogen flow at a rate of 100 mL min^{-1} and remained in this condition for 1 hour. The activation was reached by an exchange of the nitrogen flow with synthetic air or CO_2 at a rate of 100 mL min^{-1} for 1 hour. After cooling, the carbon was stored in sealed bottles at ambient temperature for later use.

The prepared charcoal from the coconut tree straw before activation, after activation with synthetic air and after activation with CO_2 were respectively named C_b, C_{air} and C_{CO2}. They were classified by a series of Tyler sieves for particle sizes of 0.090, 0.090-0.150 and 0.150-0.212 mm.

2.2. Characterization of adsorbents

2.2.1. Adsorption/desorption of N_2 by Brunauer-Emmett-Teller and Barrett-Joyner-Halenda methods

C_b, C_{air} and C_{CO2} were characterized by the adsorption/desorption of N_2 by the Brunauer-Emmett-Teller (*BET*) and the Barrett-Joyner-Halenda (*BJH*) methods to determine the specific surface area and the pore volume. The surface area of the materials was determined by N_2 adsorption at 77 ± 5 K on a Micromeritics ASAP 2420. Initially, a 0.2 g sample (< 0.090 mm) was pre-treated at 333 K under vacuum (DEGASS) for 3 hours.

2.2.2. X-ray diffraction

For the X-ray diffraction analysis (*XRD*), C_b, C_{air} and C_{CO2} were characterized in an X-ray diffractometer (Bruker, D8 Advance) using a Cu-Kα radiation source with a voltage of 30 kV and a current of 30 mA. Data were collected in the range of 2θ from 5° to 80° with steps of 0.05° and a step-time of 2.0 s.

2.2.3. Thermogravimetric analysis

The thermogravimetric curve was obtained in a thermobalance (Netzsch, STA 449 F3 Jupiter), under a nitrogen flow rate of 100 mL min^{-1}. An alumina crucible was used in this analysis, with a heating rate 20 K min^{-1} and a sample weight of 6.0 ± 0.5 mg under a temperature range of 313-873 K.

2.2.4. Fourier transform infrared spectroscopy

The adsorption spectra were obtained from a BRUKER spectrometer (model VERTEX 70), using the attenuated total reflection method (*ATR*). The data was collected in an in infrared region from 4000 cm^{-1} to 600 cm^{-1}, at a resolution of 2 cm^{-1}.

2.2.5. Determining the point of zero charge

The pH of point of zero charge (pH_{PZC}) was determined by measuring the pH of water before and after contact with the solid. Adsorbent (0.1 g) was added to 25 mL of water with a pH ranging from 2 to 11, which was adjusted with a pH metre (HANNA, pH 21). Hydrochloric acid 0.1 mol L^{-1} (Modern Chemistry) and sodium hydroxide 0.1 mol L^{-1} (Dynamics) were used for pH adjustment. The solutions were shaken at 300 rpm on a shaker table (IKA, KS 130 control) for 24 hours. The pH_{PZC} was

obtained by plotting (pH_{final}-$pH_{initial}$) *vs.* $pH_{initial}$, according to Regalbuto (2016).

2.3. Batch adsorption studies

The phenol solutions 1000 mg L^{-1} was prepared from crystalline phenol p.a. (carbolic acid – Dynamics, purity 99%) by dissolving 1 g in deionized water with no pH adjustment. Working solutions (5-300 mg L^{-1}) were obtained by successive dilutions.

The samples were quantified before and after contact with the adsorbents by UV-Visible Spectrometry (Thermo Scientific, Genesys 10S) at a wavelength of high absorbance of the compound (270 nm), according to Giraldo and Moreno-Piraján (2014). A calibration curve was plotted using a 1000 mg L^{-1} standard solution (Specsol, spectrophotometric standards), with the following analytical parameters: detection limit of 0.09 mg L^{-1}, quantitation limit of 0.3 mg L^{-1} and linear working range from 0.5 to 100 mg L^{-1}. Adsorption experiments were performed in a finite bath system. The best working conditions for the levels studied was defined using a 2^3 factorial design, with a central point in triplicate. The variables evaluated were: the adsorbent concentration (4; 8 and 12 gL^{-1}), particle size (<0.090; 0.090-0.150 and 0.150-0.212 mm) and stirring speed (0; 150 and 300 rpm), according Barros Neto et al., (2007). The adsorption experiments were run at a temperature range of 289±1 K on a shaker table (Incubator Shaker, SP Labor). A higher adsorption capacity q (mg g^{-1}) was obtained in the factorial design level of 4 g L^{-1}, while particle size was < 0.090 mm and 300 rpm. These conditions were used in the kinetic studies and to determine the adsorption equilibrium. Blank tests were carried out following the same procedures as used for the samples.

The amount of phenol adsorbed per mass of adsorbent (adsorption capacity, q) was calculated using Eq. (1):

$$q = \frac{(C_0 - C_f)V}{M} \quad (1)$$

where: q is the adsorption capacity (mg g^{-1}); C_0, the initial concentration of phenol (mg L^{-1}); C_f, the final concentration of phenol (mg L^{-1}); V, the volume of the solution (L); and M, the adsorbent mass (g).

2.3.1. Evaluation of the influence of the initial pH of the phenolic solution

The effect of the initial pH of the phenolic solution (100 mg L^{-1}) was investigated at pH levels from 2 to 11. The pH was adjusted using hydrochloric acid 0.1 mol L^{-1} (Modern Chemistry) and sodium hydroxide 0.1 mol L^{-1} (Dynamics) solutions. C_b, C_{air} and C_{CO2} (0.1 g) were added to 25 mL of the respective pH solutions and then shaken at 300 rpm for 6 hours at 298 ± 1 K. After reaching the contact time the samples were filtered and quantified.

2.3.2. Kinetic and adsorption equilibrium studies

According to the conditions established from the factorial design, the kinetic studies were carried out with 0.1 g of adsorbents added to 25 mL of the phenol solution at 100 mg L^{-1} in the following time intervals: 0, 1, 5, 10, 15, 30, 45, 60, 90, 120, 180, 240, 300, 360, 420, 480, 540 and 600 minutes, with a stirring speed of 300 rpm at 298 ± 1 K. After reaching the contact time, each sample was filtered and quantified. The experimental data were evaluated using the pseudo first-order, pseudo second-order and pseudo-*n*th order kinetic models, as well as the Weber-Morris model.

The Pseudo-first order (Eq. 2), Pseudo-second order (Eq. 3), Pseudo-*n*th order (Eq. 4) and Weber-Morris (Eq. 5) models were used (Tseng, 2014; Weber and Morris, 1963):

$$\frac{dq_t}{dt} = k_1(q_e - q_t) \quad (2)$$

where q_t is the quantity of the adsorbate adsorbed at time t (mg g^{-1}), t is the time (min), k_1 is the adsorption constant of the pseudo-first order equation (min^{-1}) and q_e is the quantity of the adsorbate adsorbed at equilibrium (mg g^{-1}).

$$\frac{dq_t}{dt} = k_2(q_e - q_t)^2 \quad (3)$$

In this equation, k_2 is the adsorption constant of the pseudo-second order equation (g mg^{-1} min^{-1}).

$$\frac{dq_t}{dt} = k_n(q_e - q_t)^n \quad (4)$$

where k_n is the adsorption constant of the pseudo-*n*th order equation (g^{n-1} g^{1-n} min^{-1}) and n is the equation order.

$$q_t = k_{dif} t^{1/2} + C \quad (5)$$

In this equation, k_{dif} is the intraparticle diffusion coefficient (mg (g $min^{0.5})^{-1}$) and C is the constant related to diffusion resistance (mg g^{-1}).

The adsorption isotherms were obtained for the range of phenol concentration 5-300 mg L^{-1}, adding 0.1 g of adsorbents with particle size <0.090 mm in a 25 mL phenolic solution, with equilibrium time defined by the kinetic study, stirred at 300 rpm at 298 ± 1 K. After reaching contact time, each sample was filtered and quantified.

The Langmuir (Eq. 6), Freundlich (Eq. 7), Fritz-Schlunder (Eq. 8), Sips (Eq. 9), Redlich-Peterson (Eq. 10) and Radke-Prausnitz (Eq. 11) equilibrium models were used according to (Giraldo and Moreno-Piraján (2014):

$$q_e = \frac{q_{max} K_L C_e}{1 + K_L C_e} \quad (6)$$

where q_{max} is the maximum quantity of the adsorbate adsorbed (mg g^{-1}), K_L is the Langmuir isotherm constants related to the energy adsorption (L mg^{-1}) and C_e is the equilibrium concentration of the adsorbate (mg L^{-1}).

$$q_e = K_F C_e^{nf} \tag{7}$$

In this equation, K_F is the Freundlich isotherm constant (mg g^{-1}) (mg L^{-1}) and nf is the adsorption intensity of the Freundlich isotherm.

$$q_e = \frac{K_{FS} C_e^{b_1}}{1 + aC_e^{b_2}} \tag{8}$$

where K_{FS} is the Fritz-Schlunder isotherm constant (mg g-1) (mg dm^{-3})$^{-b1}$; b_1 and b_2 are the heterogeneity factors of Fritz–Schlunder isotherm and a is the Fritz-Schlunder isotherm constant (mg dm^{-3})$^{-b2}$.

$$q_e = \frac{q_{\max} K_s C_e^{1/n_s}}{1 + K_s C_e^{1/n_s}} \tag{9}$$

In this equation, K_s is the Sips isotherm constant (L mg^{-1}) and n_s is the heterogeneity factor.

$$q_e = \frac{AC_e}{1 + BC_e^{g}} \tag{10}$$

where A (L g^{-1}) and B (L mg^{-1})-^{g} are Redlich-Peterson isotherm constants and g is the Redlich-Peterson isotherm exponent.

$$q_e = \frac{q_{\max} K_{RP} C_e}{(1 + K_{RP} C_e)^{m_{RP}}} \tag{11}$$

In this equation, K_{RP} is the Radke-Prausnitz isotherm constant (L g^{-1}) and m_{RP} is the Radke-Prausnitz isotherm exponent.

The mathematical models were fitted to the experimental data with a nonlinear regression method (Origin 8.0). The model parameters were obtained by minimizing the sum of squared deviations between the experimental and predicted values. The model fit was assessed by calculating the relative standard deviations (σi) and the regression coefficients (R^2). The models with the best fitting were compared using an *F test* (Montgomery, 2012). F_{cal} was calculated using Eq. (12):

$$F_{cal} = \frac{S_R^2(A)}{S_R^2(B)} \tag{12}$$

where $S_R(A)$ and $S_R(B)$ are the variances of the A and B models to $S_R(A) > S_R(B)$, respectively. If $F_{cal} > F_{tab}$, the B model shows a better fit than the A model at a 95% confidence level, with F_{tab} is the critical value tabulated value.

3. Results and discussion

3.1. Characterization of adsorbents

3.1.1. Adsorption/desorption of N_2 by Brunauer-Emmett-Teller and Barrett-Joyner-Halenda methods

The results for texture characterization by the adsorption/desorption of N_2 are shown in Table 2. Porosity is classified according to the pore size, from the International Union of Pure and Applied Chemistry (IUPAC), macro (ϕ > 500 Å), meso (20 < ϕ < 500 Å) and micropore (ϕ < 20 Å) (Thommes et al., 2015). Cb, Cair and CCO2 are classified as mesoporous.

Table 2. Results obtained by the adsorption/desorption of N_2 for C_b, C_{air} and C_{CO2}

Adsorbent	***Surface area (m^2 g^{-1})***	***Pore volume (cm^3 g^{-1})***	***Pore diameter (ϕ) (Å)***
C_b	155.7	0.03	55.2
C_{air}	178.9	0.06	57.4
C_{CO2}	258.5	0.09	58.1

The molecular size of phenol is of 7.46 Å (Lorenc-Grabowska et al., 2016), and the coals presents a pore diameter considerably higher than this, therefore enabling the access of these molecules to the coal pores. Table 2 indicates that the carbonaceous materials showed an increase in surface area, pore volume and pore diameter upon activation. According to Li et al. (2008), the activation process opens previously inaccessible pores, creates new pores and widening existing ones. Similar results were obtained by Rodrigues et al. (2011), who obtained a surface area of 206 m^2 g^{-1} and a pore volume equal to 0.1 cm^3 g^{-1} using activated carbon from avocado kernels.

3.1.2. X-ray diffraction

C_b, C_{air} and C_{CO2} had the same *XRD* pattern since they were prepared from the same agro-industrial residue. The *XRD* pattern obtained is shown in Fig. 1. Two halos were observed in Fig. 1 (at approximately 24° and 43°) and assigned to the reflections of the planes (002) and (101), indicating the formation of a crystalline carbonaceous structure. Thin peaks indicate the presence of crystalline particles in the material, which is waste produced in the carbonization process. C_b, C_{air} and C_{CO2} had predominantly an amorphous structure with a positive property for adsorbents. Similar results were obtained for activated carbons prepared from lotus stalks (Huang et al., 2011), jatropha curcas fruit shell (Tongpoothorn et al., 2011) and olive stones (Bohli et al., 2015).

3.1.3. Thermogravimetric analysis

The thermogravimetric analysis of C_b was made in order to determine the temperature at which the activation should occur, and to evaluate the thermal stability of C_{air} and C_{CO2}. The

thermogravimetric analysis (TG) curves for C_b, C_{air} and C_{CO2} are shown in Fig. 2. C_b, C_{air} and C_{CO2} showed three weight losses, two quite obvious and one less so, as shown in Fig. 2. The first weight loss occurred below 150°C, due to the loss of hygroscopic water, the second weight loss between 150°C and 400°C was related to the degradation of surface oxygen groups on carbon.

The third weight loss was due to carboxyl groups, considered less stable, decomposing at 400°C. C_{CO2} showed higher thermal stability with a residual weight of 88% at 580°C, while C_b had a residual weight of 76% and C_{air} had 80%. Both C_{CO2} and C_{air} were more thermally stable in relation to C_b, probably due to the fact that the activation occurred above 580 °C. This result corroborates that obtained by Vargas et al. (2011), in which the TG showed three weight losses for the activated carbon Flamboyant (*Delonix regia*) pods.

3.1.4. Fourier transform infrared spectroscopy

The infrared spectra from the adsorbents C_b, C_{air} and C_{CO2} before and after the adsorption are presented in Fig. 3. The spectra showed that the adsorbent functional groups display approximately the same frequency before and after the adsorption procedure. For the pre-adsorption spectrum, a band at between 3,700 and 2,700 cm^{-1} was observed, which can be due to the presence of functional groups associated with the –OH group: phenols, alcohols and carboxylic acids. The band comprised at between 1,739 and 1,515 cm^{-1} can be associated with the C=O bond stretching, present in the carbonyl groups, in carboxylic acids, and C=C bonds in olefinic and aromatic structures. The band at the region between 1,535 and 1,330 cm^{-1} is linked with the conjugated C=O bonds and the C-O bond stretching in carboxylic groups.

Finally, the bands at around 1,225 to 970 cm^{-1} being related with the C-O bond stretching in heterocyclic rings. Furthermore, after the adsorption, there was an increase in the transmitance in the bands from 3,700 to 2,700 cm^{-1}, and 1,739 to 1,515 cm^{-1}, and the presence of a 750 cm^{-1} peak, characteristic of phenol, derived from phenol molecules in the carbon structure. There was also an increase in the characteristic phenol bands after the adsorption process.

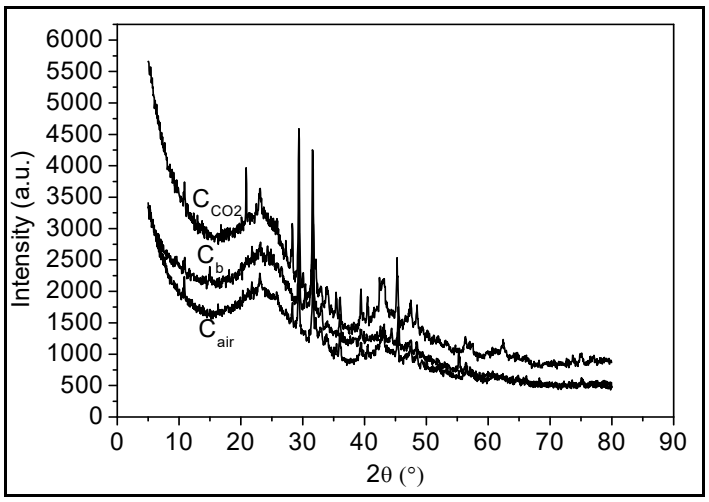

Fig. 1. X-ray diffractogram of the C_b, C_{air} and C_{CO2}

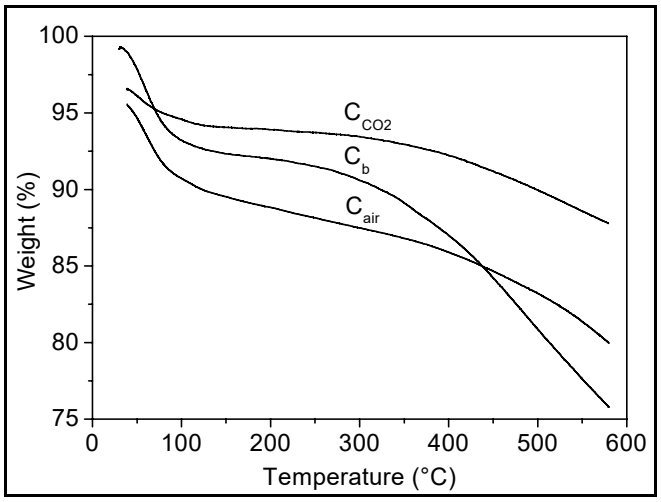

Fig. 2. *TG* curves for the adsorbents under study

3.1.5. Determining the point of zero charge

It is obvious in Fig. 4 that the C_b graph intercepted the horizontal axis at a $pH_{initial}$ of 6.4. The value of pH_{PZC} was of approximately 10.0 for both C_{air} and C_{CO2}. In solutions with a pH value less than pH_{PCZ}, the activated carbon has a positive surface charge; favouring the adsorption of compounds such as phenol. Rodrigues et al. (2011), found a pH_{PZC} value of 9.7 for carbon activated with CO_2 obtained from avocado seeds.

3.2. Batch adsorption studies

3.2.1. Evaluation of the influence of the initial pH of the phenolic solution

The adsorption capacity of C_b, C_{air} and C_{CO2} studied with respect to the different values of the $pH_{initial}$ of the phenolic solution is shown in Fig. 5. The Figure indicates that C_b showed a higher adsorption at pH 6; there was a decrease in the adsorption capacity from pH 6 to 2 that can be explained by an increase of H^+ ions, which compete for carbonyl sites, thereby suppressing the adsorption of phenol on these sites. On the other hand, phenol is a weak acid, with a p_{Ka} of approximately 9.89, dissociating at high pH values to form phenolate anions.

The excess negative charge on the adsorbent surface repels phenolate ions, thereby causing a decrease in the adsorption capacity (Atieh, 2014; El-Naas et al., 2010; Mubarik et al., 2012), as observed in Fig. 5 to C_b.

For the activated carbons C_{air} and C_{CO2}, no significant variations in the adsorption of phenol at different pH of the phenolic solution were observed because the pH values tested were below the pH_{PZC} equal to 10. Similar behaviour was observed by Dursun et al. (2005), for the adsorption of phenol on carbonised beet pulp. Subsequent experiments were performed at pH 6, as the pH of the phenolic solution must be less than the pH_{PZC}.

3.2.2. Adsorption kinetic study

Fig. 6 shows the evolution of the kinetic curves for phenol adsorption by C_b, C_{air} and C_{CO2} and adjusted by pseudo-first order, pseudo-second order, and pseudo-*n*th order non-linear kinetic models. The kinetic evolution was rapid during the initial minutes due to the greater availability of active sites; the availability of the sites decreases with time and reaches saturation equilibrium. There was a marked initial kinetic progression with most of the phenol being removed before 120 minutes. After wards, a slow step and equilibrium of approximately 300 minutes followed. In an experiment by Hameed and Rahmam (2008) using activated carbon from rattan sawdust for phenol adsorption, equilibrium was reached at 240 minutes, when initial concentrations of 25-150 mg L^{-1} of phenol were employed.

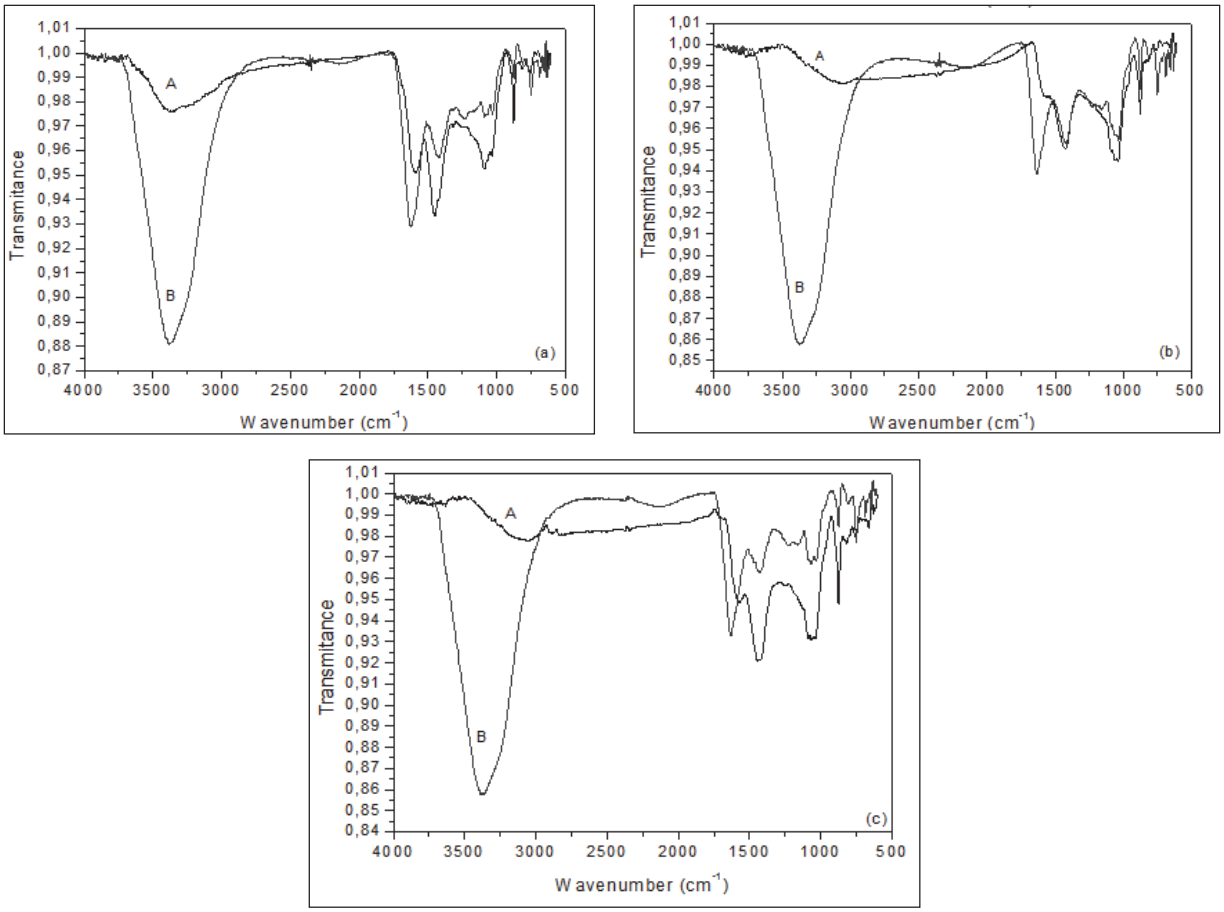

Fig. 3. FT-IR spectra of the adsorbents before (A) and after the adsorption (B): (a) - C_b; (b) - C_{air} and (c) - C_{CO2}

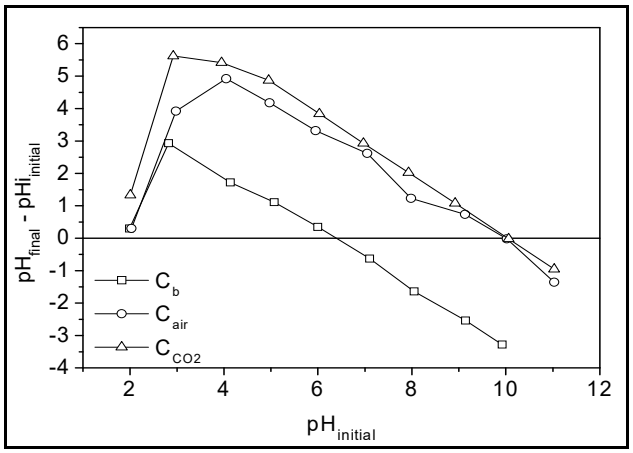

Fig. 4. Point of zero charge. pH 2 to 11, *SS* = 300 rpm and *t* = 24 h

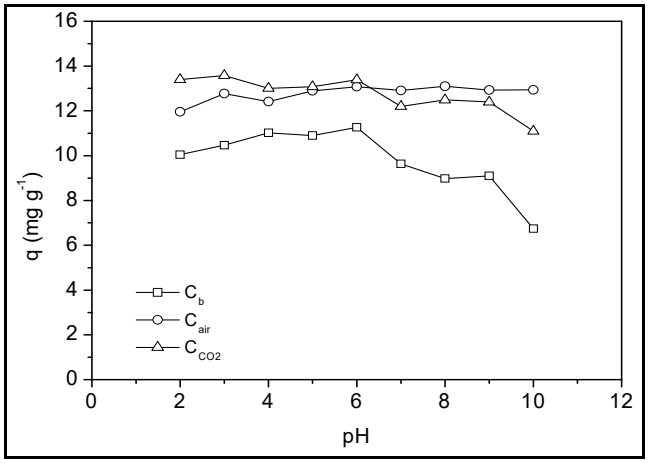

Fig. 5. Effect of the initial pH of the phenolic solution. pH 2 to 10, C_0 = 100 mg L^{-1}

The kinetic parameters calculated via the different models for C_b, C_{air} and C_{CO2} used for the adsorption of an aqueous phenol solution are shown in Table 3, where q_{ecalc} is the quantity of the adsorbate adsorbed at equilibrium calculated by the model (mg g^{-1}). According to the results obtained from an *F test* at a confidence level of 95% (Table 3), the pseudo-*n*th order model ($F_{cal} > F_{tab}$) showed the best fit to the experimental data. Pseudo-first order and pseudo-second order models did not fit the experimental data (R^2, Table 3). For the pseudo-first order model, the value obtained for k_1 did not represent the number of sites available; with q_{ecal} not being close to the experimental value, according to Han et al. (2015).

Although the R^2 was higher for the pseudo-second order model, there was no determinant relation between the initial concentration of phenol and the reaction rate constant, k_2. Fig. 6 shows an accentuation of the curvature in pseudo-*n*th order model, suggesting a higher adsorption rate. According to Tseng et al. (2014), this kinetic behaviour is best explained by pseudo-*n*th order curves rather than pseudo-first and pseudo-second order curves. For values of $n > 2$, Tseng et al. (2014) suggest that the adsorption rate increases proportionally with the value of *n*.

The Weber-Morris model (Fig. 7), a plot of q_t *vs.* $t^{1/2}$, shows the relationship between the amount adsorbed and time. This model allows the evaluation of the kinetic adsorption mechanism. According to Yousef et al. (2011), if intraparticle diffusion occurs, then q_t is a linear function of $t^{1/2}$, and the curve passes through the origin. Otherwise, some other mechanism controls the process. The multi-linear nature of the data (Fig. 7) indicates that two or more steps with different rate constants affect the adsorptive process, being necessary to evaluate each linear region separately, according to Tang et al (2012). According to Sousa Neto et al. (2011), the first straight line corresponds to the diffusion of the molecule of solute in the boundary layer, with the second to the intraparticle diffusion and the third characterising the final equilibrium phase. Linear adjustments were made for three regions.

The parameters of the Weber-Morris kinetic model are shown in Table 4. The intraparticle diffusion constant decreases with time (Table 4), indicating that the intraparticle diffusion decreases as the carbon adsorbs molecules, because of the low concentration of adsorbate in the solution, according to Arthy and Saravanakumar (2013). According to Yousef et al. (2011), a mechanism other than intraparticle diffusion controls the process, as the plotted curves do not pass through the origin. The *F test* results (F_{cal} (Table 5) < F_{tab} (3.18)) at a 95%

confidence level indicate no significant differences among the Fritz-Schlunder, Redlich-Peterson, Radke-Prausnitz and Sips models for C_b, C_{air} and C_{CO2}. The two-parameter models (Langmuir and Freundlich) did not fit the experimental data well (R^2 <0.99) and had higher variances than the models with more parameters. The Langmuir model is considered valid for the adsorption in homogeneous surfaces. As the coals studied presented superficial heterogeneity (functional groups observed in the FT-IR, impurities in the DRX, as well as the n_s heterogeneity factor of Sips under 1), the Freundlich model obtained the best adjustment in relation to the Langmuir model (Table 5); once the latter is better adjusted on heterogeneous surfaces.

Table 3. Kinetic parameters calculated via different models for the C_b, C_{air} and C_{CO2} used for the adsorption of phenol

Models	***Parameters***	***C_b***	***C_{air}***	***C_{CO2}***
[1]Pseudo-first Order	$q_{ecalc.}$ (mg g^{-1})	11.74 ± 0.67	15.10 ± 0.73	17.31 ± 0.78
	k_1 (min^{-1})	0.025 ± 0.007	0.09 ± 0.03	0.13 ± 0.04
	S_R^2 (mg^2 g^{-2})	56.80	96.32	115.33
	R^2	0.732	0.730	0.735
[2]Pseudo-second Order	$q_{ecalc.}$(mg g^{-1})	12.51 ± 0.70	16.27 ± 0.70	18.32 ± 0.72
	k_2 (g mg^{-1} min^{-1})	0.004 ± 0.001	0.006 ± 0.002	0.009 ± 0.003
	S_R^2(mg^2 g^{-2})	36.74	54.88	69.81
	R^2	0.826	0.846	0.840
[3]Pseudo *n*th Order	q_{ecalc} (mg g^{-1})	15.31 ± 0.48	19.01 ± 0.38	21.20 ± 0.47
	K_n (g^{n-1} mg^{1-n} min^{-1})	8.85 10^{-5} ± 1.98 10^{-5}	7.04 10^{-5} ± 1.67 10^{-5}	4.42 10^{-5} ± 1.44 10^{-5}
	n	2.44 ± 0.03	2.58 ± 0.04	2.70 ± 0.05
	S_R^2 (mg^2 g^{-2})	1.73	2.51	4.70
	R^2	0.985	0.986	0.976
F Test	$F_{cal\ (1/2)}$	1.54	1.75	1.65
	$F_{cal\ (1/3)}$	32.80	38.37	24.53
	$F_{cal\ (2/3)}$	21.23	21.86	14.85
	F_{tab}	2.14	2.14	2.14

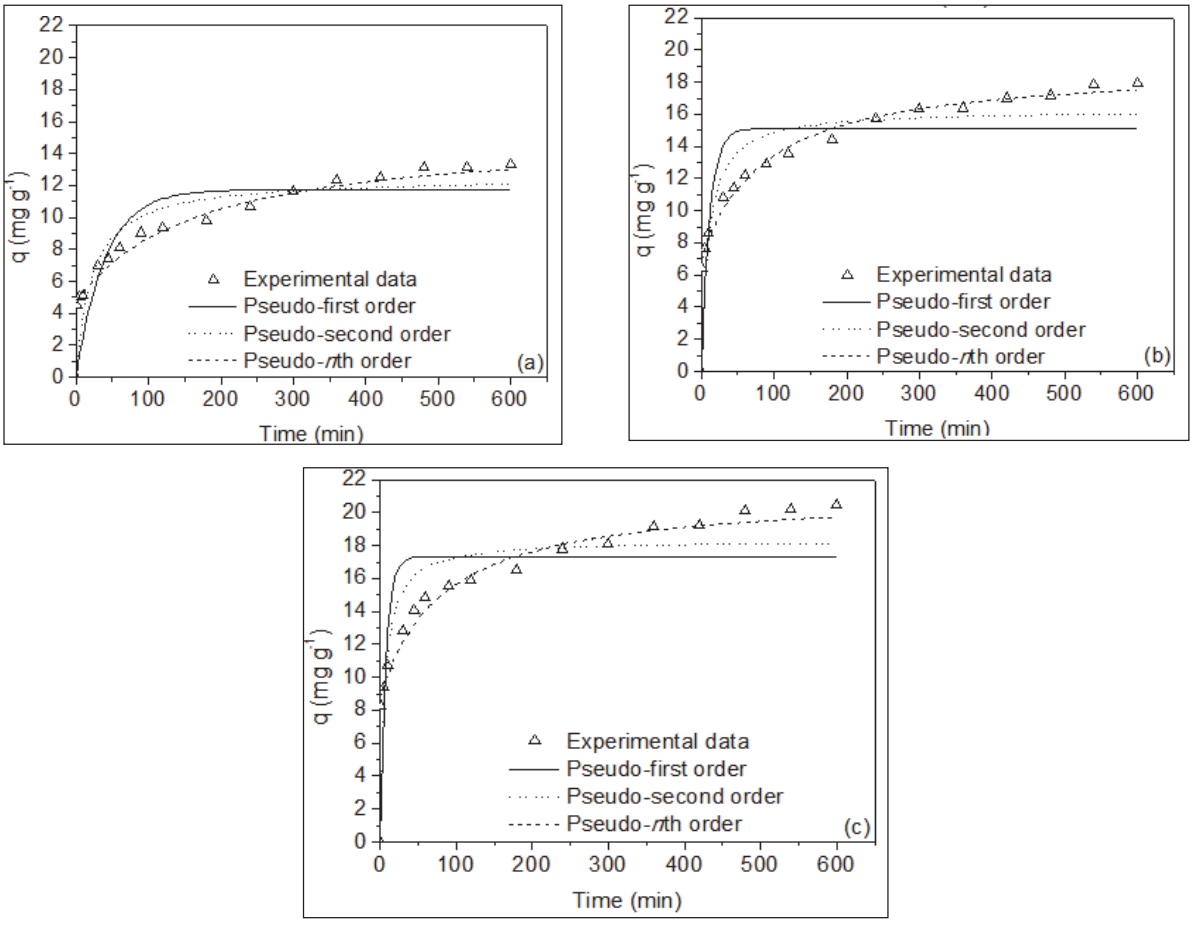

Fig. 6. Adsorption kinetics in a finite bath with nonlinear kinetic models of system settings. (a) - C_b; (b) - C_{air} and (c) - C_{CO2}. pH = 6.0, SS = 300 rpm, PS < 0.090 mm and AC = 4 g L^{-1}

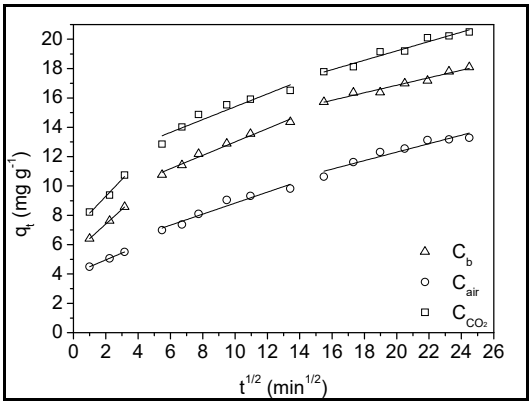

Fig. 7. Intraparticle diffusion model of Weber-Morris. pH = 6.0, *SS* = 300 rpm, *PS* < 0.090 mm and *AC* = 4 g^{-1}

The Redlich-Peterson, Radke-Prausnitz, Sips and Fritz Schlunder models are also applicable for describing the adsorption in heterogeneous surfaces, and include more than two parameters; these models better representing the adsorption of phenol for the coals studied (Table 5). According Subramanyam and Ashutosh (2012), models with more parameters better adjust to the experimental data, for example, the Fritz-Schlunder model showed a lower variance (S_R^2) for all of the coals.

The adsorption capacity increased by 27% after activation using synthetic air and 73% using CO_2, demonstrating that activation with CO_2 was more effective than that with synthetic air, probably due to the increased formation of oxygen functional groups on the carbon surface. The adsorption capacity increased by 27% after activation using synthetic air and 73% using CO_2, demonstrating that activation with CO_2 was more effective than that with synthetic air, probably due to the increased formation of oxygen functional groups on the carbon surface. We compared the efficiencies of C_b, C_{air} and C_{CO2} from this study with other results for different types of adsorbents used to remove phenolic compounds from aqueous solutions that were reported in the literature (Table 6).

The data indicated that activated carbons from the coconut tree straw present good efficiency compared to results found for other activated carbons in the literature.

Table 4. The intraparticle diffusion model parameters of Weber-Morris

Parameters	***C_b***	***C_{air}***	***C_{CO2}***
$k_{dif,1}$ **mg (g min$^{0.5}$)$^{-1}$**	0.998 ± 0.014	0.467 ± 0.060	1.154 ± 0.150
C_1 **(mg g^{-1})**	5.412 ± 0.033	4.028 ± 0.013	6.988 ± 0.348
R_1^2	0.999	0.999	0.966
$k_{dif,2}$ **mg (g min$^{0.5}$)$^{-1}$**	0.456 ± 0.030	0.376 ± 0.045	0.438 ± 0.069
C_2 **(mg g^{-1})**	8.444 ± 0.278	5.073 ± 0.424	11.025 ± 0.645
R_2^2	0.979	0.931	0.887
$k_{dif,3}$ **mg (g min$^{0.5}$)$^{-1}$**	0.256 ± 0.021	0.289 ± 0.037	0.319 ± 0.028
C_3 **(mg g^{-1})**	11.744 ± 0.426	6.531 ± 0.759	12.816 ± 0.578
R_3^2	0.962	0.909	0.955

Table 5. Isotherm parameters for phenol on an adsorbent obtained by non-linear methods at 298 K

Charcoal coconut tree straw without activation (C_b)		
Langmuir	***Freundlich***	***Sips***
q_{max} (mg g^{-1}) = 20.1 ± 1.2	K_F (mg g^{-1}) = 2.4 ± 0.3	q_{max} (mg g^{-1}) = 32 ± 6
K_L (L g^{-1}) = 0.031 ± 0.006	n = 2.6 ± 0.2	K_s (L mg^{-1})$^{-1/n}$ = 0.008 ± 0.005
R^2 = 0.9701	R^2 = 0.9814	n_s = 0.60 ± 0.07
S_R^2 (mg^2 g^{-2}) = 7.91	S_R^2 (mg^2 g^{-2}) = 4.93	R^2 = 0.9927
		S_R^2 (mg^2 g^{-2}) = 1.70
Fritz-Schlunder	***Redlich-Peterson***	***Radke-Prausnitz***
K_{FS} (mg g^{-1}) (mg dm^{-3})$^{-b_1}$ = 1.8 ± 0.8	A (L g^{-1}) = 1.9 ± 0.6	q_{max} (mg g^{-1}) = 5 ± 1
a (mg dm^{-3})$^{-b_2}$ = 0.5 ± 0.3	B (L mg^{-1})^g = 0.4 ± 0.2	K_{RP} (L g^{-1}) = 0.3 ± 0.1
b_1 = 1.2 ± 0.5	g = 0.72 ± 0.04	m_{RP} = 0.69 ± 0.03
b_2 = 0.9 ± 0.5	R^2 = 0.9939	R^2 = 0.9939
R^2 = 0.9931	S_R^2 (mg^2 g^{-2}) = 1.41	S_R^2 (mg^2 g^{-2}) = 1.41
S_R^2 (mg^2 g^{-2}) = 1.38		
Activated carbon from coconut tree straw ***activated by synthetic air (C_{air})***		
Langmuir	***Freundlich***	***Sips***
q_{max} (mg g^{-1}) = 26 ± 1	K_F (mg g^{-1}) = 6.2 ± 0.6	q_{max} (mg g^{-1}) = 41 ± 6
K_L (L g^{-1}) = 0.09 ± 0.02	n = 3.4 ± 0.2	K_s (L mg^{-1})$^{-1/n}$ = 0.02 ± 0.01
R^2 = 0.9536	R^2 = 0.9760	n_s = 0.51 ± 0.05
S_R^2 (mg^2 g^{-2}) = 28.05	S_R^2 (mg^2 g^{-2}) = 14.51	R^2 = 0.9934
		S_R^2 (mg^2 g^{-2}) = 3.48
Fritz-Schlunder	***Redlich-Peterson***	***Radke-Prausnitz***

K_{FS} (mg g^{-1}) (mg dm^{-3})$^{-b_1}$ = 5.1 ± 0.4	A (L g^{-1}) = 13 ± 6	q_{max} (mg g^{-1}) = 7 ± 2
a (mg dm^{-3})$^{-b_2}$= 0.002 ± 0.001	B (L mg^{-1})^{g} = 2 ± 1	K_{RP} (L g^{-1}) = 2 ± 1
b_1 = 0.38 ± 0.05	g = 0.77 ± 0.03	m_{RP} = 0.75 ± 0.03
b_2 = 1.0 ± 0.6	R^2 = 0.9886	R^2 = 0.9869
R^2 = 0.9936	S_R^2 (mg^2 g^{-2}) = 6.05	S_R^2 (mg^2 g^{-2}) = 6.93
S_R^2 (mg^2 g^{-2}) = 2.90		
Activated carbon from coconut tree straw ***activated by CO_2 (C_{CO2})***		
Langmuir	***Freundlich***	***Sips***
q_{max} (mg g^{-1}) = 35 ± 2	K_F (mg g^{-1}) = 6.7 ± 0.3	q_{max} (mg g^{-1}) = 56 ± 7
K_L (L g^{-1}) = 0.07 ± 0.02	n = 3.0 ± 0.2	K_s (L mg^{-1})$^{-1/n}$ = 0.014 ± 0.007
R^2 = 0.9577	R^2 = 0.9801	n_s = 0.54 ± 0.04
S_R^2 (mg^2 g^{-2}) = 41.32	S_R^2 (mg^2 g^{-2}) = 19.47	R^2 = 0.9957
		S_R^2 (mg^2 g^{-2}) = 3.68
Fritz-Schlunder	***Redlich-Peterson***	***Radke-Prausnitz***
K_{FS} (mg g^{-1}) (mg dm^{-3})$^{-b_1}$= 5.6 ± 0.9	A (L g^{-1}) = 10 ± 3	q_{max} (mg g^{-1}) = 9 ± 2
a (mg dm^{-3})$^{-b_2}$= 0.10 ± 0.05	B (L mg^{-1})^{g} = 1.1 ± 0.5	K_{RP} (L g^{-1})= 0.9 ± 0.4
b_1 = 0.5 ± 0.1	g = 0.75 ± 0.02	m_{RP} = 0.73 ± 0.02
b_2 = 0.6 ± 0.2	R^2 = 0.9942	R^2 = 0.9932
R^2 = 0.9950	S_R^2 (mg^2 g^{-2})= 4.96	S_R^2 (mg^2 g^{-2})= 5.83
S_R^2 (mg^2 g^{-2})= 3.67		

Table 6. Summary of values of adsorptive capacity for activated carbons found in the literature

Adsorbent	***C_o (mg L^{-1})***	***q_{max} (mg g^{-1})***	***Reference***
Activated carbon from coconut shell by thermally activation in inert atmosphere	75	34	Singh et al., 2008
Activated carbon from piassava fibres by activation with CO_2	1000	138	Avelar et al., 2010
Activated carbon from avocado kernel seeds activated by CO_2	600	90	Rodrigues et al., 2011
Activated carbon from sawdust *Eucalyptus* sp. activated by CO_2	1000	172	Couto et al., 2012
Charcoal straw coconut tree straw without activation	300	32	This study
Activated carbon from straw coconut tree straw activated by synthetic air	300	41	This study
Activated carbon from straw coconut tree straw activated by CO_2	300	56	This study

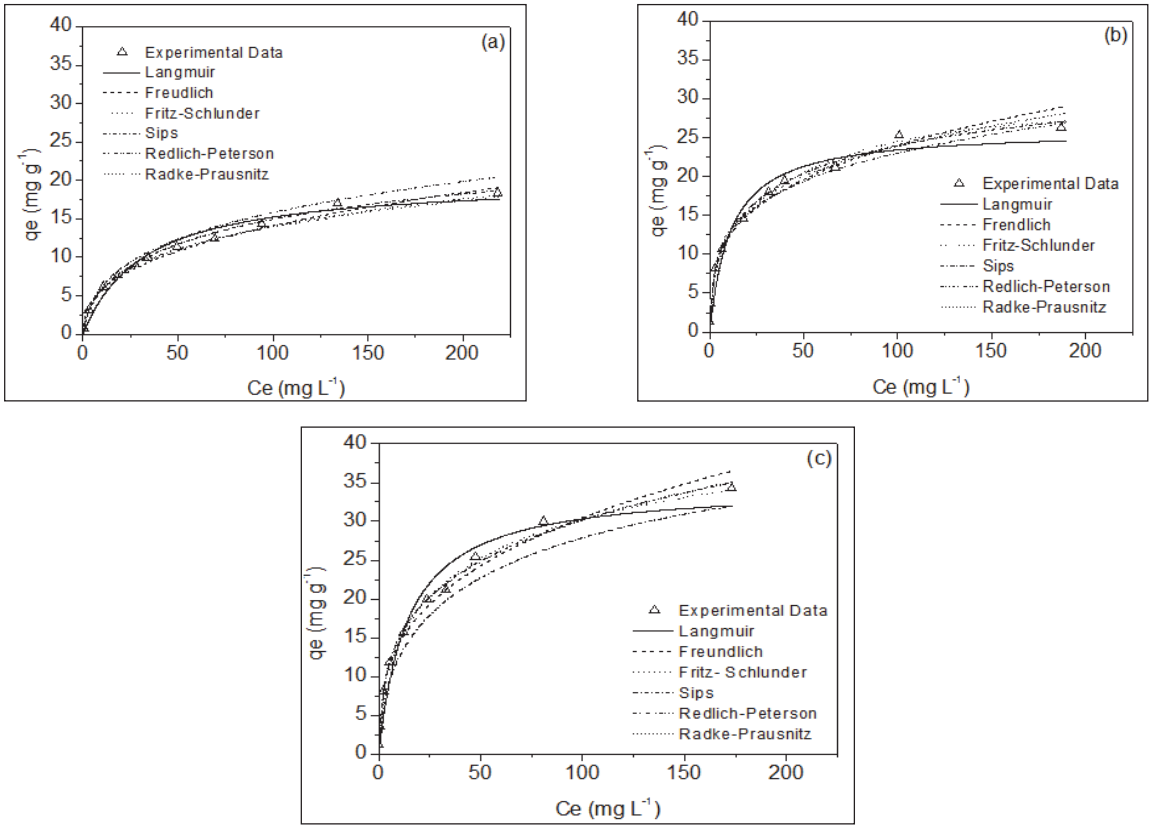

Fig. 8. Adsorption isotherms in a finite bath system with nonlinear adjustment models.
(a) - C_b; (b) - C_{air} and (c) - C_{CO2}. pH = 6.0, SS = 300 rpm, PS < 0.090 mm and AC = 4 g L^{-1}

4. Conclusions

The activation method with synthetic air or CO_2 employed to obtain the activated carbons from the coconut tree straw was efficient because the adsorptive capacity increased de 32 mg L^{-1} for 41 mg L^{-1} and 56 mg L^{-1}, respectively.

The adsorbents were characterized as mesoporous with an amorphous structure, and the thermogravimetric analysis showed three mass losses. The activation shifted the pH_{PZC} to pH 10, increasing the band at which the coal surface was positively charged and favouring the adsorption of compounds such as phenol.

In the kinetic study it was concluded that the equilibrium time was reached in 240 minutes. The pseudo-*n*th order model provided the best fit for the kinetic data, within the three models evaluated. The Weber-Morris model indicated that the adsorption process is controlled by more than one step, once the data presented multilinear nature; indicating that the process is controlled by the diffusion of the solute molecule in the boundary layer, by the intraparticle diffusion and by the final phase of equilibrium.

No significant differences were observed among the Fritz-Schlunder, Redlich-Peterson, Radke-Prausnitz and Sips models for the adsorption equilibrium, according to an *F test* at the 95% confidence level.

The coals prepared from the coconut tree straw presented a better performance after activation. The activated coal with CO_2 was considered the most efficient adsorbent for the removal of phenol, in relation to the other adsorbents evaluated in this study.

The use of activated carbon prepared from the residue of the coconut tree straw as an adsorbent for the removal of phenolic compounds from industrial effluents is both technically feasible and environmentally advantageous.

Acknowledgments

The authors would like to thank ANP, PETROBRAS, FINEP and NUQAAPE/FACEPE, for providing the financial resources needed for this work. The authors are also thankful to Elephant Chemical Industry Ltda. for donating the charcoal straw coconut tree straw, CETENE, and providing help with the characterization of adsorbents.

References

Ageitec, (2010), Technology Information Embrapa Agency (in Portuguese), On line at: http://www.agencia.cnptia.embrapa.br/gestor/coco/arvore/CONT000giw3qz5o02wx5ok05vadr1u5iye30.html

Almasi A., Dargahi A., Amrane A., Fazlzadeh M., Soltanian M., Hashemian A., (2018), Effect of molasses addition as biodegradable material on phenol removal under anaerobic conditions, *Environmental Engineering and Management Journal*, **17**, 1475-1482.

Arthy M., Saravanakumar M.P., (2013), Isotherm modeling, kinetic study and optimization of batch parameters for effective removal of Acid Blue 45 using tannery waste, *Journal of Molecular Liquids*, **187**, 189-200.

Atieh M.A., (2014), Removal of phenol from water different types of carbon - a comparative analysis, *APCBEE Procedia*, **10**, 136-141.

Avelar F.F., Bianchi M.L., Gonçalves M., Mota E.G., (2010), The use of piassava fibers (*Attalea funifera*) in the preparation of activated carbon, *Bioresource Technology*, **101**, 4639-4645.

Barros Neto B., Scarminio I.S., Bruns R.E. (2007), How do experiments: Research and development in science and industry (in Portuguese), Unicamp Press, Campinas-São Paulo.

Bohli T., Ouederni A., Fiol N., Villaescusa I., (2015), Evaluation of an activated carbon from olive stones used as an adsorbent for heavy metal removal from aqueous phases, *Comptes Rendus Chimie*, **18**, 88-99.

Britto J.M., Rangel M.C., (2008), Advanced Oxidation Process of phenolic compounds in industrial wasterwater, *Química Nova*, **31**, 114-122.

Couto G.M., Dessimoni A.L.A., Bianchi M.L., Perígolo D.M., Trugilho P.F., (2012), Use of sawdust eucalyptus sp. in the preparation of activated carbons, *Ciência e Agrotecnologia*, **36**, 69-77.

Couto Jr O. M., Matos I., Fonseca I.M., Arroyo P.A., Silva E.A., Barros M.A.S.D., (2015), Effect of solution pH and influence of water hardness on caffeine adsorption onto activated carbons, *The Canadian Journal of Chemical Engineering*, **93**, 68-77.

Dursun G., Çiçek H., Dursun A.Y., (2005), Adsorption of phenol from aqueous solution by using carbonized beet pulp, *Journal of Hazardous Materials*, **125**, 175-182.

El-Naas M.H., Al-Zuhair S., Alhaija M.A., (2010), Removal of phenol from petroleum refinery wastewater through adsorption on date-pit activated carbon, *Chemical Engineering Journal*, **162**, 997-1005.

Fu Y., Shen Y., Zhang Z., Ge X., Chen M., (2019), Activated bio-chars derived from rice husk via one- and two-step KOH-catalyzed pyrolysis for phenol adsorption, *Science of the Total Environment*, **646**, 1567-1577.

Gama B.M.V., Nascimento G.E., Sales D.C.S., Rodríguez-Díaz J.M., Barbosa C.M.B.M, Duarte M.M.M., (2018), Mono and binary component adsorption of phenol and cadmium using adsorbent derived from peanut shells, *Journal of Cleaner Production*, **201**, 219-228.

Giraldo L., Moreno-Piraján J.C., (2014), Study of adsorption of phenol on activated carbons obtained from eggshells, *Journal of Analytical and Applied Pyrolysis*, **106**, 41-47.

Gundogdu A., Duran C., Senturk H.B., Soylak M., Ozdes D., Serencam H., Imamoglu M., (2012), Adsorption of phenol from aqueous solution on a low-cost activated carbon produced from tea industry waste: equilibrium, kinetic and thermodynamic study, *Journal of Chemical & Engineering Data*, **57**, 2733-2743.

Hameed B.H., Rahman A.A., (2008), Removal of phenol from aqueous solutions by adsorption onto activated carbon prepared from biomass material, *Journal of Hazardous Materials*, **160**, 576-581.

Han J., Du Z., Zou W., Li H., Zhang C., (2015), In-situ improved phenol adsorption at ions enrichment interface of porous adsorbent for simultaneous removal of copper ions and phenol, *Chemical Engineering Journal*, **262**, 571-578.

Huang L., Sun Y., Wang W., Yue Q., Yang T., (2011), Comparative study on characterization of activated carbons prepared by microwave and conventional heating methods and application in removal of oxytetracycline (OTC), *Chemical Engineering Journal*, **171**, 1446-1453.

Instituto Brasileiro de Geografia e Estatística - IBGE (2017). Levantamento Sistemático da Produção Agrícola. **30**, 1-81.

Jun T.Y., Arumugam S.D., Latip N.H.A., Abdullah A.M., Latif P.A., (2010), Effect of activation temperature and heating duration on physical characteristics of activated carbon prepared from agriculture waste, *Environment Asia*, **3**, 143-148.

Karri R.R., Sahub J.N., Jayakumar N.S., (2017), Optimal isotherm parameters for phenol adsorption from aqueous solutions onto coconut shell based activated carbon: Error analysis of linear and non-linear methods, *Journal of the Taiwan Institute of Chemical Engineers*, **80**, 472–487.

Karthikeyan S., Gopalakrishnan A.N., (2017), Effect of microwaves on photocatalytic degradation of phenol and cresols in a microwave-ultraviolet reactor, *Environmental Engineering and Management Journal*, **16**, 285-292.

Kulkarni S.J., Tapre R.W., Patil S.V., Sawarkar M.B., (2013), Adsorption of phenol from wastewater in fluidized bed using coconut shell activated carbon, *Procedia Engineering*, **51**, 300-307.

Lekene N.R.B., Kouoh S.P.M.A., Ndi N.J., Kouotou D., Belibi B.P.D., Ketcha M.J., (2015), Kinetics and equilibrium studies of the adsorption of phenol and methylene blue onto cola nut shell based activated carbon, *International Journal of Current Research and Review*, **7**, 1-9.

Li W., Yang K., Peng J., Zhang L., Guo S., Xia H., (2008), Effects of carbonization temperatures on characteristics of porosity in coconut shell chars and activated carbons derived from carbonized coconut shell chars, *Industrial Crops and Products*, **28**, 190-198.

Lorenc-Grabowska E., Diez M.A., Gryglewicz G., (2016), Influence of pore size distribution on the adsorption of phenol on PET-based activated carbons, *Journal of Colloid and Interface Science*, **469**, 205–212.

Luo X., Chen X., Liu L., Feng Y., Li B., Guo J., (2017), Performance of modified bentonites for adsorption of phenol: mechanisms, kinetics and isotherms, *Environmental Engineering and Management Journal*, **16**, 2505-2511

Martins C.R., Jesus Júnior L.A., (2014), Production and marketing of coconut in Brazil over international trade: Panorama 2014 (in Portuguese), *Embrapa Tabuleiros Costeiros*, **184**, 1-51.

Montgomery D.C., (2012), *Introduction to Statistical Quality Control* (in Portuguese), 4th Edition, Livros Técnicos e Científicos Editora, Rio de Janeiro, Brasil..

Mubarik S., Saeed A., Mehmood Z., Iqbal M., (2012), Phenol adsorption by charred sawdust of sheesham (Indian rosewood; *Dalbergia sissoo*) from single, binary and ternary contaminated solutions, *Journal of the Taiwan Institute of Chemical Engineers*, **43**, 926-933.

Păcurariu C., Mihoc G., Popa A., Muntean S. G., Ianoş R., (2013), Adsorption of phenol and p-chlorophenol from aqueous solutions on poly (styrene-co-divinylbenzene) functionalized materials, *Chemical Engineering Journal*, **222**, 218-227.

Regalbuto J., (2016), Catalyst preparation: Science and engineering, CRC Press, New York, 2016.

Rincón-Silva N.G., Moreno-Piraján J.C., Giraldo L.G., (2015), Thermodynamic study of adsorption of phenol, 4-chlorophenol, and 4-nitrophenol on activated carbon obtained from eucalyptus seed, *Journal of Chemistry*, **2015**, 1-12.

Rodrigues L.A., da Silva M.L.C.P., Alvarez-Mendes M.O., Coutinho A.R., Thim G.P., (2011), Phenol removal from aqueous solution by activated carbon produced from avocado kernel seeds, *Chemical Engineering Journal*, **174**, 49-57.

Saraç N., Uğur A., Şimşek Ö., Aytar P., Toptaş Y., Buruk Y., Çabuk A., Burnak N., (2017), Phenol tolerance and biodegradation optimization of Serratia marcescens NSO9-1 using Plackett-Burman and Box-Behnken design, *Environmental Engineering and Management Journal,* **16**, 2637-2645.

Secula M.S., Dávid E., Cagnon B., Vajda A., Stan C., Mămăligă I., (2018), Kinetics and equilibrium studies of 4-chlorophenol adsorption onto magnetic activated carbon composites, *Environmental Engineering and Management Journal*, **17**, 783-793.

Sellaoui L., Kehili M., Lima E.C., Thue P.S., Bonilla-Petriciolet A., Lamine A.B., Dotto G.L., Erto A., (2019), Adsorption of phenol on microwave-assisted activated carbons: Modelling and interpretation, *Journal of Molecular Liquids*, **274**, 309-314.

Singh K.P., Malik A., Sinha S., Ojha P., (2008), Liquid-phase adsorption of phenols using activated carbons derived from agricultural waste material, *Journal of Hazardous Materials*, **150**, 626-641.

Soto M.L., Moure A., Domínguez H., Parajó J.C., (2011), Recovery, concentration and purification of phenolic compounds by adsorption: A review, *Journal of Food Engineering*, **105**, 1-27.

Sousa Neto V.O., Oliveira A.G., Teixeira R.N.P., Silva M. A.A., Freire P.C.T., Keukeleire D.D., Nascimento R.F., (2011), Use of coconut bagasse as alternative adsorbent for separation of copper (II) ions from aqueous solutions: isotherms, kinetics, and thermodynamic studies, *Bioresources Technology*, **6**, 3376-3395.

Sun J., Liu X., Zhang F., Zhou J., Wu J., Alsaedi A., Hayat T., Li J., (2019), Insight into the mechanism of adsorption of phenol and resorcinol on activated carbons with different oxidation degrees, *Colloids and Surfaces A*, **563**, 22-30.

Subramanyam B., Ashutosh D., (2012), Adsorption isotherm modeling of phenol onto natural soils-applicability of various isotherm models, *International Journal of Environmental Research*, **6**, 265-276.

Tang B., Lin Y., Yu P., Luo Y., (2012), Study of aniline/ε-caprolactam mixture adsorption from aqueous solution onto granular activated carbon: Kinetics and equilibrium, *Chemical Engineering Journal*, **187**, 69-78.

Thommes M., Kaneko K., Neimark A.V., Olivier J.P., Rodriguez-Reinoso F., Rouquerol J., Sing K.S.W. (2015), Physisorption of gases, with special reference to the evaluation of surface area and pore size distribution (IUPAC Technical Report), *Pure and Applied Chemistry*, **87**, 1051-1069.

Tongpoothorn W., Sriuttha M., Homchan P., Chanthai S., Ruangviriyachai C., (2011), Preparation of activated carbon derived from *Jatropha curcas* fruit shell by simple thermo-chemical activation and characterization of their physico-chemical properties, *Chemical Engineering Research and Design*, **89**, 335-340.

Tseng R.-L., Wu P.-H., Wu F.-C., Juang R.-S., (2014), A convenient method to determine kinetic parameters of adsorption processes by nonlinear regression of pseudo-nth-order equation *Chemical Engineering Journal*, **237**, 153-161.

Vargas A.M.M., Cazetta A.L., Garcia C.A., Moraes J.C.G., Nogami E.M., Lenzi E., Costa W.F., Almeida V.C., (2011), Preparation and characterization of activated

carbon from a new raw lignocellulosic material: Flamboyant (*Delonix regia*) pods, *Journal of Environmental Management*, **92**, 178-184.

Weber W.J., Morris J.C., (1963), Kinetics of adsorption carbon from solutions, *Journal of the Sanitary Engineering Division*, **89**, 31-60.

Yousef R.I., El-Eswed B., Al-Muhtaseb A.H., (2011), Adsorption characteristics of natural zeolites as solid adsorbents for phenol removal from aqueous solutions: kinetics, mechanism, and thermodynamics studies, *Chemical Engineering Journal*, **171**, 1143-1149.

Zhang D., Huo P., Liu W., (2016), Behavior of phenol adsorption on thermal modified activated carbon, *Chinese Journal of Chemical Engineering*, **24**, 446–452.